



# CHORUS

This is the accepted manuscript made available via CHORUS. The article has been published as:

## From cells to tissue: A continuum model of epithelial mechanics

Shuji Ishihara, Philippe Marcq, and Kaoru Sugimura

Phys. Rev. E **96**, 022418 — Published 31 August 2017

DOI: [10.1103/PhysRevE.96.022418](https://doi.org/10.1103/PhysRevE.96.022418)

# From cells to tissue: A continuum model of epithelial mechanics

Shuji Ishihara\*

*Graduate School of Arts and Sciences, The University of Tokyo, Tokyo 153-8902, Japan and  
Department of Physics, School of Science and Technology, Meiji University, Kanagawa 214-8571, Japan*

Philippe Marcq

*Sorbonne Universités, UPMC Université Paris 6, Institut Curie,  
CNRS, UMR 168, Laboratoire Physico Chimie Curie, Paris, France*

Kaoru Sugimura

*Institute for Integrated Cell-Material Sciences (WPI-iCeMS), Kyoto University, Kyoto 606-8501, Japan and  
JST PRESTO, Tokyo 102-0075, Japan*

(Dated: August 16, 2017)

A two-dimensional continuum model of epithelial tissue mechanics was formulated using cellular-level mechanical ingredients and cell morphogenetic processes, including cellular shape changes and cellular rearrangements. This model incorporates stress and deformation tensors, which can be compared with experimental data. Focusing on the interplay between cell shape changes and cell rearrangements, we elucidated dynamical behavior underlying passive relaxation, active contraction-elongation, and tissue shear flow, including a novel mechanism for contraction-elongation whereby tissue flows perpendicularly to the axis of cell elongation. This study provides an integrated scheme for the understanding of the orchestration of morphogenetic processes in individual cells in order to achieve epithelial tissue morphogenesis.

## I. INTRODUCTION

During tissue morphogenesis, tissues acquire their unique shape and size through a series of deformations. Morphogenesis occurs at multiple levels, and molecular, cellular, and tissue level changes are interdependent. At cellular level, tissue deformation is accounted for by changes in cell shape, position, and number (Fig. 1(a); hereafter named cell morphogenetic processes), which are triggered by biochemical signaling and forces generated by cells [1–3]. While the tissue stress can affect cell morphogenetic processes through the changes in molecular activity and localization, cell morphogenetic processes generate stress [4–10]. However, the mechanisms by which the shape of a tissue emerges from these multi-scale feedback processes remain unclear.

In order to clarify this, a coarse-grained description and modeling of cellular and tissue dynamics at an appropriate length scale is required: while the position and timing of cell morphogenetic processes are stochastic at single cell level, the averaging of values obtained over a larger length scale yields a smooth spatial pattern that is reproducible among different samples. We previously determined the appropriate averaging length scale for describing epithelial tissue dynamics (several tens of cells in a patch), and developed coarse-grained methods for measuring stress and kinematics [11–14]. A force inference method was used for the quantification of cell junction tensions and cell pressures (Fig. 1(b), (c)), which can be integrated to calculate a stress tensor [13–16]. A texture

tensor method was used for the measuring of different cell morphogenetic processes (*e.g.*, cell division, cell shape changes) in the same physical dimension, which can be further integrated to obtain tissue scale, spatio-temporal maps of tissue growth and cell morphogenetic processes [12]. Together, these methods provide the information on the amplitude, orientation, and anisotropy of tissue stress, tissue growth, and cell morphogenetic processes, and correlations between them [12].

A modeling scheme capable of accommodating the quantitative data described above is still lacking [17]. Cell-based models, such as the cell vertex model (CVM) [18], the cellular Potts model (CPM) [19], particle-based models [20–22] and phase-field models [23–25], explicitly consider a cellular shape. Among them, the CVM and CPM are often employed for the simulation of epithelial tissue morphogenesis (Fig. 1(d); [26–28]), and have proven useful for including experimental data obtained at cellular level, such as the laser ablation of cell junctions or subcellular distribution of proteins. However, the relationship between cell morphogenetic processes and tissue scale deformation and rheology emerges from numerical simulations without being directly tractable. Continuum models allow the in-depth analysis of tissue rheology [29, 30], yet in many cases do not include the information of the cellular structure by construction, and thus fail to discriminate between different cell morphogenetic processes. A limited number of studies considered the degrees of freedom that represent cell morphogenetic processes and cell polarity [30–33], but do so in the context of macroscopic models, which do not incorporate cell-level mechanical parameters explicitly. The finite-element model introduced in [34] includes at a coarse-grained level the contributions of cellular rhe-

---

\* csishihara@g.ecc.u-tokyo.ac.jp

ology, shape changes, rearrangements and divisions. A continuum model has been derived from the CVM previously but without considering cell rearrangements [35] (see also [36, 37] in 1D).

The main aim of this study was to develop a two-dimensional hydrodynamic model of the epithelial tissue. This model included a field that represents coarse-grained cell shape, which enabled us to treat different types of cell morphogenetic processes distinctively. First, kinematics was identified by decomposing tissue deformation into cell shape changes and topological transitions. Following this, by introducing an energy function deduced from CVM/CPM, thermodynamic formalism was employed to determine kinetics. The model we derived here describes tissue deformation through stress and deformation tensors, which can be compared with the data obtained experimentally [12–14], and can incorporate active terms smoothly. We solved the model for several conditions typical for deforming planar tissues during development, and demonstrated that the model predicts the relaxation of cellular shape following the tissue stretching, the relation of the direction of cell elongation and tissue flow during active contraction-elongation (CE), and shear-thinning in tissues. Our approach provides a theoretical framework that enables to assess how cellular level mechanical parameters and cell morphogenetic processes are integrated to realize tissue-scale deformation.

## II. MODEL

### A. Kinematics

#### 1. Cellular shape tensor

To construct a continuum model, we characterized each cell shape by using a  $2 \times 2$  symmetric tensor  $M$ , with the unit of square length, which can be the texture matrix [12], the gyration tensor of cellular mass, or can simply be obtained by fitting the cell by an ellipse. With appropriate scaling, each cell shape is quantified by the expression  $(\vec{r} - \vec{r}_c)^T M^{-1} (\vec{r} - \vec{r}_c) = 1$  (Fig. 1(e)), where  $\vec{r}_c$  represents the center of a cell and superscript  $T$  denotes the transpose. Since the eigenvalues of  $M$  may be seen as the square lengths of ellipse semi-axes, cell area can be computed as  $A = \pi |M|^{1/2}$ , where  $|M|$  is the determinant of  $M$ . By coarse-graining over a representative surface element comprising a sufficient number of cells [11, 12], we obtained a spatially smooth tensor field  $M(\vec{r})$ . Similar to the previously described texture tensor [12], the symmetric tensor  $M(\vec{r})$  represents measure of tissue scale deformation in our model, which can be experimentally quantified from segmented images of two-dimensional (2D) epithelia. In the following, all fields that we introduce are obtained by similar coarse-graining, see [11, 12] for details of the practical implementation on experimental data.

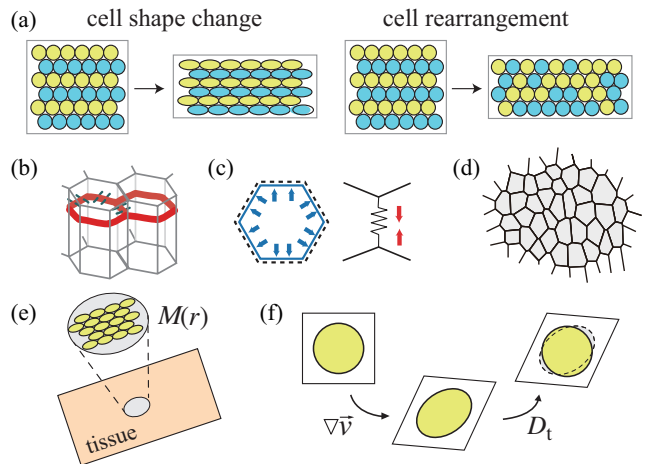


FIG. 1. Schematic illustration of the model of epithelial mechanics. (a) Tissue deformation based on cellular shape deformation (left) and by cellular rearrangement (right). (b) In epithelial tissues, cells adhere to each other via E-Cadherin (green) at adherens junctions (AJ), and actomyosin (red) runs along the cell junctions. (c) Cell pressures (left) and cell junction tensions (right) act in the AJ plane and determine epithelial cell shapes. (d) CVM schematic representation. Each cell is represented by a polygonal contour. (e, f) Schematic illustration of the model presented here. (e) A coarse-grained cellular shape tensor  $M$  represents the tissue-scale cellular shape field in our model. (f) Kinematics of cellular shape deformation. Cellular shape alterations through tissue deformation  $\nabla \vec{v}$  and topological changes in a network of cellular junctions  $D_t$ , such as cell rearrangement, division, and death.

#### 2. Kinematic relationship

Total tissue deformation rate can be represented by the tensor  $\nabla \vec{v}$ , in which  $\vec{v}$  is the velocity field. Here, we used  $(\nabla \vec{v})_{ij} = \partial_j v_i$ , where indices  $i$  and  $j$  denote cartesian coordinates. The deformation rate  $\nabla \vec{v}$  represents the sum of its symmetric part  $D = (\nabla \vec{v} + [\nabla \vec{v}]^T)/2$  and its antisymmetric part  $\Omega = (\nabla \vec{v} - [\nabla \vec{v}]^T)/2$ . We decomposed tissue deformation rate into the sum of contributions, due to the cellular shape alterations and other cell morphogenetic processes, and here, we considered cell rearrangement, division, and death:

$$\nabla \vec{v} = \Omega + D_s + D_t. \quad (1)$$

The quantity  $\Omega + D_s$  represents the tissue deformation rate stemming from cellular shape alterations, while  $D_t$  denotes the deformation rates that involve topological changes in a network of cell junctions, *i.e.* cell rearrangement, division, and death. We assumed that these processes are irrotational, so that  $D_t$  is symmetric. In practice, these tensors can be experimentally determined by cellular shape tracking. Using notations defined in [12],  $D_s$  corresponds to the tensor  $S$  that quantifies the rate of cell size and shape changes, and  $D_t$  corresponds to the sum  $R + D + A$  of contributions due to cell rear-

rangements  $R$ , cell divisions  $D$ , and apoptoses  $A$ .

Since cells adhere tightly to each other in an epithelial tissue, cell shape changes are kinematically associated with tissue deformation as [30]

$$\frac{dM}{dt} - (\nabla\vec{v} - D_t)M - M(\nabla\vec{v} - D_t)^T = 0, \quad (2)$$

where  $dM/dt \equiv \partial_t M + \vec{v} \cdot \nabla M$  represents the Lagrange derivative of  $M$  (Fig. 1(f)). When  $D_t = 0$ , the left-hand side of Eq. (2) becomes the co-deformational upper-convected derivative [38, 39]. The kinematic relationship Eq. (2) was derived in the case of non-affine deformations in the rheology of polymer melts [40–42] where  $D_t$  was interpreted as due to the slippage between polymer molecules. An underlying assumption for Eq. (2) to hold is that the velocity field be sufficiently smooth [43] (see [30, 43–45] for derivations of (2) in the context of cellular materials). As shown below, the kinematic relationship Eq. (2) leads to a cell number balance equation (Eq. (4) in Sec. II A 3) and an elastic stress tensor (Eq. (5) in Sec. II B 1; see Appendix A 1), which contrasts with another type of a kinematic equation employed in earlier study [33].

### 3. Cell number balance equation

The balance equation for cell number density is obtained from the above kinematic relationship. From Eq. (2), we calculate

$$\frac{d}{dt}|M| = 2|M|(\nabla \cdot \vec{v} - \text{Tr } D_t), \quad (3)$$

where  $\text{Tr}$  denotes the trace. The cell number density field  $\rho$  is defined by  $\rho = 1/\pi|M|^{1/2}$ , and its evolution equation reads

$$\frac{\partial\rho}{\partial t} + \nabla \cdot (\rho\vec{v}) = [\text{Tr } D_t]\rho. \quad (4)$$

We identify  $\text{Tr } D_t$  as the variation rate of the cell number density.

Although the effects of cell division and cell death should be investigated in future studies, here we considered a situation in which individual cells only deform elastically and/or intercalate. Hence, in this work, the deformation rate involving topological change  $D_t$  is identical to that by cell rearrangement (intercalation)  $D_r$ . Through cell rearrangement the tissue area is invariant and the deformation rate is traceless ( $\text{Tr } D_r = 0$ ), by which Eq. (4) becomes the conservation equation for cell number density.

## B. Energy function and ground state

### 1. Energy function and elastic stress in an isotropic tissue

The energy functions introduced in cell-based models depend on all cell configurations and include cell mechan-

ical properties, such as cell elasticity, cell adhesion and cell-interface contractility. In our continuum model, we introduce the tissue energy function  $\tilde{F} = \int F d\vec{r}$ , where  $F$  is the energy density per unit area. In the case of a two-dimensional, isotropic tissue without any signal that indicates orientational information,  $F$  is a function of the invariants  $|M|$  and  $\text{Tr } M$ .

For a given energy density  $F(M)$ , the elastic stress is obtained by

$$\sigma_e = FI + \left(\frac{\partial F}{\partial M}\right)^T M + \left(\frac{\partial F}{\partial M}\right) M^T, \quad (5)$$

where  $I$  is the unit tensor (see Appendix A 1). When the tissue is isotropic and  $\partial F/\partial M$  and  $M$  commute, Eq. (5) further simplifies to

$$\begin{aligned} \sigma_e &= FI + 2\left(\frac{\partial F}{\partial M}\right)M \\ &= \left(F + 2\frac{\partial F}{\partial|M|}|M|\right)I + 2\left(\frac{\partial F}{\partial\text{Tr } M}\right)M, \end{aligned} \quad (6)$$

for which we used the relations  $\partial\text{Tr } M/\partial M = I$  and  $\partial|M|/\partial M = |M|M^{-1}$ . Since higher-order terms proportional to  $M^n$  ( $n \geq 2$ ) can be eliminated by using the Cayley-Hamilton formula in 2D, the elastic stress of an isotropic tissue is expressed as

$$\sigma_e = -\Pi(|M|, \text{Tr } M)I + \Sigma(|M|, \text{Tr } M)M', \quad (7)$$

where  $\Pi(M)$  and  $\Sigma(M)$  are scalar functions of  $|M|$  and  $\text{Tr } M$ , and  $X' \equiv X - (\text{Tr } X/2)I$  denotes the deviatoric part of an arbitrary tensor  $X$ . The first and second terms in Eq. (7) represent isotropic and deviatoric elastic stresses, respectively.

### 2. Energy function deduced from the CVM/CPM

In the CVM and CPM, cell geometry can be determined by minimizing energy function [26, 46]

$$f_c = \sum_i \frac{K}{2} (A_i - A_0)^2 + \sum_{[ij]} \gamma_0 \ell_{ij} + \sum_i \frac{\kappa_0}{2} L_i^2, \quad (8)$$

where  $A_i$  and  $L_i$  represent the area and perimeter, respectively, of cell  $i$ , and  $\ell_{ij}$  is the length of the interface between cells  $i$  and  $j$ . The first term represents cell-area elasticity with elastic modulus  $K$  and reference cell area  $A_0$ . The second and third terms represent cell junction tensions, where the tension is given by  $\gamma_0 + \kappa_0(L_i + L_j)$ .

Here, by using the cell shape tensor  $M(\vec{r})$ , we considered an energy function for the continuum model, which is comparable with that of the CVM/CPM, Eq. (8). For arbitrary semi-axes  $a$ ,  $b$ , the perimeter of an ellipse can be given by Euler's formula (see Fig. S1 in Appendix [47]):

$$L(a, b) = \pi \sqrt{2(a^2 + b^2)} \mathcal{F}\left(\frac{1}{4}, -\frac{1}{4}; 1; h^2\right), \quad (9)$$

where  $h = (a^2 - b^2)/(a^2 + b^2)$  and  $\mathcal{F}$  is a hypergeometric function. Using the Cayley-Hamilton equation, we derived the identities  $a^2 + b^2 = \text{Tr } M$ ,  $(a^2 - b^2)^2 = \text{Tr } M^2 - 4|M|$ . Upon coarse-graining Eq. (8), we obtained energy density per unit area

$$F = \frac{1}{\pi|M|^{1/2}} \left[ \frac{K}{2} (\pi|M|^{1/2} - A_0)^2 + \frac{\gamma_0}{2} L(M) + \frac{\kappa_0}{2} L(M)^2 \right], \quad (10)$$

where  $L(M)$  is defined for arbitrarily large cellular shape

$$F = \frac{1}{\pi|M|^{1/2}} \left[ \frac{K}{2} (\pi|M|^{1/2} - A_0)^2 + \frac{\pi\gamma_0}{\sqrt{2}} \sqrt{\text{Tr } M} + \pi^2 \kappa_0 \text{Tr } M \right], \quad (12)$$

from which the elastic stress can be further derived as

$$\sigma_e = K(\pi|M|^{1/2} - A_0)I + \left( \frac{\gamma_0}{\sqrt{2}\text{Tr } M} + 2\pi\kappa_0 \right) \frac{M}{|M|^{1/2}}. \quad (13)$$

The first and second terms represent the isotropic pressure  $-P^{ce}I$  due to the area-elasticity of cells, and the cellular shape-dependent stress  $\sigma^T$  due to cell junction tensions, respectively. Eq. (13) is consistent with the expression of the Batchelor stress tensor [13, 14, 48] relating tissue-scale stress to cell pressures and cell junction tensions. Note that  $\sigma_e$  and  $M$  commute, and therefore, share the same eigendirections, which is consistent with our previous observation showing that cells are elongated along the inferred maximal stress direction in *Drosophila* epithelia [6, 12, 13].

We performed numerical simulation of the CVM under the isotropic and anisotropic stress environments, and compared the coarse-grained stress with the true one (see Appendix A 2 for details). Coarse-grained cell shape  $M$  was evaluated by averaging the second moment of cell shape, and Euler expansion up to the second order was considered. The results obtained here confirmed that the coarse-grained stress values agree with those obtained for the true one (Fig. 2(a,b) and Fig. S2 in Appendix).

### 3. Ground states of the system

Factorizing the tensor  $M$  as  $M = M_0 e^{c\Theta}$  can be useful [49], and here,  $M_0$  and  $c$  are scalar fields and  $\Theta$  is a symmetric, trace-less tensor field parameterized by the angle  $\theta$  as

$$\Theta = \begin{pmatrix} \cos 2\theta & \sin 2\theta \\ \sin 2\theta & -\cos 2\theta \end{pmatrix}. \quad (14)$$

Since  $\Theta^2 = I$ , we deduced  $M = M_0[\cosh(c)I + \sinh(c)\Theta]$ , where  $M_0$  quantifies the coarse-grained cell area  $A = \pi|M|^{1/2} = \pi M_0$ , dimensionless parameter  $c$  characterizes

anisotropy by

$$L(M) = \pi \sqrt{2\text{Tr } M} \mathcal{F} \left( \frac{1}{4}, -\frac{1}{4}; 1; 1 - \frac{4|M|}{(\text{Tr } M)^2} \right). \quad (11)$$

The total elastic energy  $\tilde{F}$  was obtained by integration  $\tilde{F} = \int F(M(\vec{r})) d\vec{r}$ .

We focused, for simplicity, on conditions close to the isotropic case (see Appendix A 2 for higher-order approximations). Expanding  $\mathcal{F}$  close to  $a = b$ , or  $(\text{Tr } M)^2 = 4|M|$ , the zero order energy can be written as

the coarse-grained cell shape anisotropy, and the angle  $\theta$  represents the direction of the major axis of ellipses. Since  $\text{Tr } M = 2M_0 \cosh(c)$ ,  $L(M)$  and  $F(M)$  depend only on  $M_0$  and  $c$ .

For the energy function presented in Eq. (12), the energy per cell,  $AF(A, c = 0)$ , is shown as a function of  $A$  in Fig. 2(c) in the isotropic case  $c = 0$ . For large values of  $\gamma_0$ , the functional form becomes concave, indicating thermodynamic instability of the state of homogeneous cell area. Fig. 2(d) shows  $F(A, c)$  as a function of  $c$  at constant cell area. Circular cell shape ( $c = 0$ ) becomes unstable for sufficiently large negative values of  $\gamma_0$ , where cells no longer prefer a hexagonal configuration, but adopt an elongated shape. We recovered two instabilities described for the CVM [46, 50] (Fig. 2(e); Appendix A 3), showing that the tissue scale energy density  $F(M)$  retains the essential features of the original cell-based models.

## C. Thermodynamic formalism

### 1. Thermodynamic formalism and activities

Since existing cell-based models, including the CVM and CPM, use *ad hoc* prescriptions for kinetics, we considered the thermodynamic formalism [51] in order to derive generic hydrodynamic equations. We decompose the total stress tensor  $\sigma$  into elastic stress  $\sigma_e$  and inelastic stress  $\sigma_p$  as

$$\sigma = \sigma_e + \sigma_p, \quad (15)$$

where  $\sigma_p$  is determined below. The entropy production rate of an isothermal process was calculated as [41, 42]

$$T\dot{s} = \sigma : D - \sigma_e : D_s = \sigma_p : D + \sigma_e : D_r, \quad (16)$$

where  $s$  is the entropy density, and  $T$  is the temperature. Here,  $a:b \equiv \text{Tr}[ab^T]$  denotes the scalar product

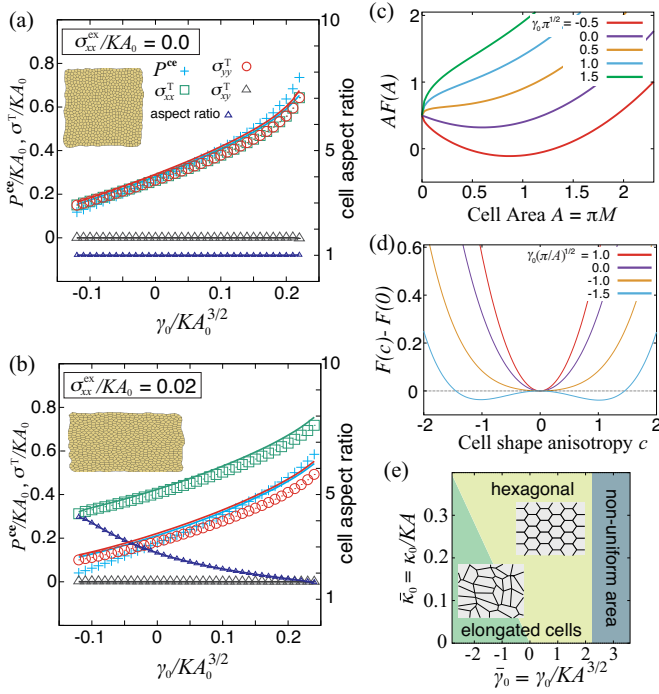


FIG. 2. Energy function and elastic stress. (a,b) Macroscopic stress expressions calculated from coarse-grained cellular shape tensor  $M$  (symbols) are compared with the true ones (solid lines) obtained using the CVM simulations (left vertical axis), as a function of the non-dimensional parameter  $\gamma_0/K_0 A_0^{3/2}$ , with  $\kappa_0/K_0 A_0 = 0.04$ .  $P^{ce}$  and  $\sigma^T$  represent the pressure stemming from cell elasticity and the stress generated by cell junction tensions, respectively. Blue triangles denote the mean cellular shape aspect ratio (right vertical axis), equal to  $e^{2c}$  in terms of the cell shape anisotropy. The external stress was set as  $\sigma_{xy}^{ex} = \sigma_{yy}^{ex} = 0$ , with (a)  $\sigma_{xx}^{ex} = 0$  (isotropic case) and (b)  $\sigma_{xx}^{ex} \neq 0$  (anisotropic case). A green solid line overlaps with a red line in (a). (c) Energy per cell as a function of the cell area  $A$  at  $\gamma_0 \pi^{1/2} = -0.5, 0.0, 0.5, 1.0$  and  $1.5$  with  $K = 1.0$  and  $2\pi\kappa_0 = 0.4$ . (d) Energy density function  $F(c)$  at  $\gamma_0(\pi/A)^{1/2} = 1.0, 0.0, -1.0$ , and  $-1.5$  with  $2\pi\kappa_0/A = 0.6$ . (e) A ground state phase diagram is shown as a function of non-dimensional parameters  $\bar{\gamma}_0 = \gamma_0/K_0 A^{3/2}$  and  $\bar{\kappa}_0 = \kappa_0/K_0 A$ , defined using a cell area  $A = \pi M_0$ , instead of  $A_0$ .

of two arbitrary tensors  $a$  and  $b$ . Because  $D_r$  is traceless, we can replace  $\sigma_e$  by  $\sigma_e'$  in Eq. (16). By identifying conjugate flux-force pairs as  $\sigma_p \cdot D$  and  $D_r \cdot \sigma_e'$ , the fluxes ( $\sigma_p, D_r$ ) can be given by using the linear combinations of the forces ( $D, \sigma_e'$ ):

$$\sigma_p = \chi^{ss} D - \chi^{sr} \sigma_e', \quad (17)$$

$$D_r = \chi^{rs} D + \chi^{rr} \sigma_e'. \quad (18)$$

The coefficients  $\chi^{ss}, \chi^{sr}, \chi^{rs}$ , and  $\chi^{rr}$  are fourth-order tensors that satisfy Onsager's reciprocity (e.g.,  $\chi_{ijkl}^{sr} = \chi_{klij}^{rs}$ ), and must be chosen to satisfy  $\text{Tr} D_r = 0$  in Eq. (18). Diagonal terms  $\chi^{ss} D$  and  $\chi^{rr} \sigma_e'$  are dissipative terms, for which Maxwell's model is obtained at

$\chi^{ss} = \chi^{sr} = 0$  ( $\sigma = \sigma_e, \sigma_p = 0$ ), and Kelvin-Voigt's model is obtained at  $\chi^{rs} = \chi^{rr} = 0$  ( $D = D_s, D_r = 0$ ) [41, 42]. The term  $\chi^{ss} D$  characterizes dissipative stress due to the tissue strain rate, and reduces to the usual bulk and shear viscous terms for isotropic material. The terms  $-\chi^{sr} \sigma_e'$  and  $\chi^{sr} D$  are reactive, representing slippage among cells (see below) and do not contribute to the entropy production. According to Eq. (18), cell rearrangements may be driven both by the tissue strain rate and by its elastic stress [5, 6, 52].

In the absence of external forces, the above equations can predict the relaxation to the steady state, and are not sufficient to address the active phenomena, such as the sustained epithelial flow [53] or self-organized spatio-temporal patterning [54]. Therefore, we included the formalism of active gels [55, 56], and added the term  $r \Delta\mu$  to the entropy production rate Eq. (16):

$$T \dot{s} = \sigma_p : D + \sigma_e' : D_r + r \Delta\mu, \quad (19)$$

where  $\Delta\mu$  represents the change in chemical potential associated with a chemical reaction that supplies energy to the system, and  $r$  is the reaction rate. By identifying  $r \cdot \Delta\mu$  as an additional force-flux pair, additional terms  $\sigma_a$  and  $D_a$ , which we refer to as active stress and active cell rearrangement, appeared in Eqs. (17) and (18), both of which are proportional to  $\Delta\mu$ .

## 2. Constitutive relations

With the condition that  $D_r$  is traceless, the simplest form of the force-flux relationships can be written as:

$$\sigma_p = \eta D' + \eta' (\text{Tr} D) I - \nu_1 \sigma_e' - \zeta_1 \Delta\mu I - \zeta_2 \Delta\mu M', \quad (20)$$

$$D_r = \nu_1 D' + \eta_1^{-1} \sigma_e' - \beta_2 \Delta\mu M', \quad (21)$$

where the coupling coefficients are scalar in an isotropic system. In Eq. (20),  $\eta$  and  $\eta'$  denote the tissue shear and bulk viscosity, respectively. The term  $\nu_1 D'$  of Eq. (21) plays a role similar to that of the Gordon-Schowalter process in the rheology of polymer melts [39]. Assuming  $\nu_1 > 0$ , it describes a process in which cells slip with respect to each other at a rate proportional to the tissue deformation rate, whereas the term  $-\nu_1 \sigma_e'$  in Eq. (20) indicates a consequent stress reduction. In Eq. (20), we introduced the active stress tensor as  $\sigma_a = -(\zeta_1 I + \zeta_2 M') \Delta\mu$ . Using the terminology of active nematic liquid crystals, a negative and positive  $\zeta_2$  values correspond to a contractile and extensile, respectively, material [56]. These activities are often attributed to myosin contractility, for which ATP is consumed. More generally, all coupling coefficients may depend on  $M'$ , see Appendix B 1 for a generalization of Eqs. (20-21) including lowest-order nonlinearities. The term coupling  $D_r$  and  $\sigma_e'$  in Eq. (21) underlies the Maxwellian dynamics of the system, and include the positive coefficient  $\eta_1$  with the dimension of viscosity. In Eq. (21), active cell rearrangements contribute

to the constitutive equation for  $D_r$  as  $D_a = -\beta_2 \Delta \mu M'$ . Both  $\sigma_a$  and  $D_a$  are symmetric second-order tensors. Our treatment of active stresses and active cell rearrangements was similar to that suggested previously [33, 52], since both approaches are inspired by the active gel models [55, 56].

Finally, the force balance equation was used to close the system:

$$\nabla \cdot \sigma = -\vec{f}_{\text{ex}}, \quad (22)$$

where  $\vec{f}_{\text{ex}}$  represents the external force field, supplemented with the appropriate boundary conditions. Collectively, the constitutive equations (Eqs. 13, 15, 20, 21) with the kinematic relationships (Eqs. 1, 2) and the force balance equation Eq. (22) determine hydrodynamic equations of a tissue.

### III. APPLICATIONS

We investigated three simple examples of dynamical behavior predicted by our model, including the passive response following the axial stretch induced by an external force, the deformation of a tissue due to the active internal forces, and the generation of shear flow. Two assumptions were used for simplicity to obtain the following analytical solutions: 2D incompressibility of a tissue ( $M_0$  is constant and  $\text{Tr} D = \text{div} \vec{v} = 0$ ; Appendix B 2) and spatial homogeneity of all relevant fields.

#### A. Passive relaxation following the axial stretching

In *Drosophila* pupal wing, an external force from the proximal part of the body is responsible for the stretching of the wing along the proximal-distal (PD) axis. Upon the tissue stretching, wing cells elongate along the PD axis, while the tissue relaxes during several hours when cells intercalate and adopt a less elongated shape [5, 6, 12, 52]. Below, we demonstrated that our model can recapitulate this process, and determined the characteristic relaxation time in terms of cell mechanical parameters.

We considered a tissue with an initial size  $l_x \times l_y = l_0 \times l_0$  and in an initial isotropic, uniform state where the cell shape tensor is  $M = M_0 I$ . From time  $t = 0$ , the tissue elongates along the  $x$ -axis at the constant rate  $\dot{l}_x/l_x = \partial_x v_x = \lambda$ , and consequently, contracts along the  $y$ -axis at the rate  $\dot{l}_y/l_y = \partial_y v_y = -\lambda$  (Fig. 3(a)). When the tissue size reaches  $\alpha l_0 \times \alpha^{-1} l_0$ , the stretching stops ( $\partial_x v_x = \partial_y v_y = 0$ ). We attempted to identify a uniform solution to the problem, so that Eq. (22) is automatically verified when  $f_{\text{ex}} = 0$ . All tensor variables are diagonal ( $M = M_0 e^{c\Theta}$  with  $\theta = 0$ ). Since we consider a passive process here and ignore active terms, we set  $\Delta \mu = 0$ . Using Eq. (2), the time evolution of  $c$  can be written as:

$$\dot{c} = 2(1 - \nu_1) \partial_x v_x - 2\eta_1^{-1} \Gamma(c) \sinh(c), \quad (23)$$

where  $\Gamma(c) = \gamma_0/2\sqrt{M_0 \cosh c} + 2\pi\kappa_0$  represents the strength of cell junction tensions as a function of cell mechanical parameters  $\gamma_0$  and  $\kappa_0$ . The normal stress components were

$$\sigma_{xx} = -p + \eta \partial_x v_x + (1 - \nu_1) \Gamma(c) \sinh c, \quad (24)$$

$$\sigma_{yy} = -p + \eta \partial_y v_y - (1 - \nu_1) \Gamma(c) \sinh c, \quad (25)$$

where the pressure  $p$  was determined in order to satisfy the incompressibility condition.

Setting  $\alpha = 5$ , the time course of cell shape anisotropy  $c(t)$  is presented for several values of  $\lambda$  in Figure 3(b). When  $|c| \ll 1$ , the temporal evolution becomes Maxwellian,

$$\dot{c} + 2\eta_1^{-1} \Gamma(0) c = 2(1 - \nu_1) \partial_x v_x. \quad (26)$$

This equation explicitly relates the relaxation time for cell rearrangements  $\tau_r = \eta_1/2\Gamma(0)$  to cell mechanical parameters. If the stretch rate is slower than this time scale ( $\tau_r < \lambda^{-1}$ ), the cells remain approximately circular during cell rearrangement, which is in a sharp contrast to transient cell elongation during the more rapid tissue stretch.

Given cell junction tensions of the order of  $\gamma_0 \approx 10^{-10}$  N [57], and a cellular length scale of the order of  $r \approx 10^{-6}$  m, we expected  $\Gamma(0) \sim \gamma_0/r \approx 10^{-4}$  N m $^{-1}$ . Since the time scale for relaxation is of the order of a few hours,  $\tau_r \approx 10^4$  s [5, 6], we obtained the order of magnitude of the 2D viscosity coefficient  $\eta_1 \sim \Gamma(0)\tau_r \approx 1$  Pa m s. For comparison, we expected a 2D shear viscosity of the order of  $\eta \approx 1$  Pa m s, provided by  $\eta = h \eta_{3D}$ , where  $h \approx 10^{-5}$  m represents the typical height of the epithelium and  $\eta_{3D} \approx 10^5$  Pa s was determined *in vitro* in cell aggregates [58, 59].

#### B. Active contraction-elongation (CE)

CE denotes the simultaneous shrinkage and expansion of a tissue along two orthogonal axes [60], often controlled by the anisotropic localization/activity of signaling/driving molecules, such as molecular motors [1, 3, 11, 61, 62]. During the CE, cells are often elongated along the axis perpendicular to the direction of the tissue flow (Fig. 4(a)) [60–63] which may occur in order to facilitate the force transmission along the axis of tissue contraction, through the formation of multicellular myosin cables through the mechanosensing of neighboring cells [62]. However, the mechanisms whereby tissue deformation due to the cellular shape alterations counteract that due to the cell rearrangements remain unclear.

Here, we investigated the CE by extending our model to include active stress and rearrangements provided by signaling molecules oriented along a fixed direction, as represented by a traceless tensor  $Q = \vec{n} \otimes \vec{n} - \text{Tr}(\vec{n} \otimes \vec{n})/2$ , where  $\vec{n} = (\cos \phi, \sin \phi)^T$  represents a unit vector field pointing to the direction  $\phi$ . Possible feedbacks on the

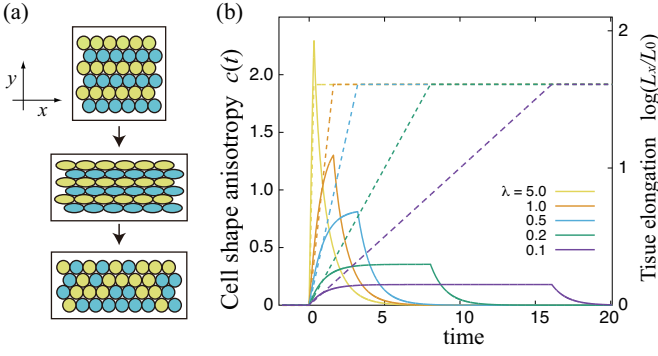


FIG. 3. Passive relaxation of cellular shape anisotropy following the tissue stretching. (a) Stretching along the  $x$ -axis of a tissue with the constant area. Cells are elongated, and after relaxation, they recover their circular shapes. (b) Cellular shape anisotropy  $c(t)$  (solid lines). Forced deformation ( $\alpha = 5$ , dashed lines) with the deformation rates  $\lambda = 5.0, 1.0, 0.5, 0.2, 0.1 \times 10^{-4} \text{ s}^{-1}$  is followed by relaxation (numerical solution of Eq. (23)). Parameters are  $\gamma_0/(4M_0)^{1/2} = 0.1 \text{ mN m}^{-1}$ ,  $2\pi\kappa_0 = 0.4 \text{ mN m}^{-1}$ ,  $\nu_1 = 0.1$ , and  $\eta_1 = 1.0 \text{ Pa m s}$ . The characteristic time  $\tau_r = \eta_1/2\Gamma(0) = 1.0 \times 10^4 \text{ s}$  is used as the time unit.

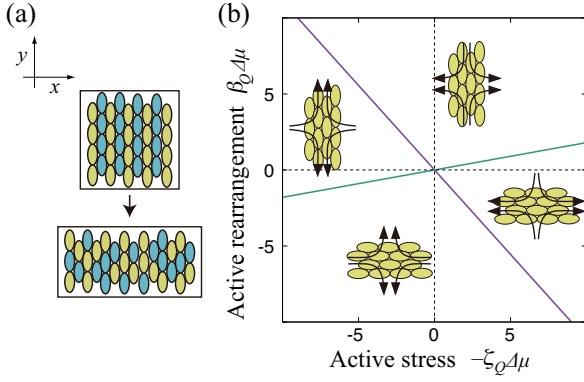


FIG. 4. Active contraction-elongation (CE) of a tissue. (a) Schematics of CE in *Xenopus* embryo [60, 61]. Due to the cell rearrangement, the tissue simultaneously shrinks along the medio-lateral,  $y$  axis and elongates along the anterior-posterior,  $x$ -axis, whereas the cells adopt an elongated shape along the  $y$ -axis. (b) Phase diagram showing the dependence of the cellular shape anisotropy  $c$  and the tissue deformation rate  $\partial_x v_x$  on the active parameters  $\zeta_Q \Delta\mu$  and  $\beta_Q \Delta\mu$ . Ellipses illustrate cellular shape, and arrows point to the direction of tissue flow. Parameter values are set as  $\nu_1 = 0.1 < 1$ ,  $\eta_1 = 1.0 \text{ Pa m s}$ , and  $\eta = 5.0 \text{ Pa m s}$ .

signal activity were ignored. We considered the lowest-order active contributions

$$\sigma_a = -\zeta_1 \Delta\mu I - \zeta_Q \Delta\mu Q, \quad (27)$$

$$D_a = -\beta_Q \Delta\mu Q, \quad (28)$$

where the parameters  $\zeta_Q$  and  $\beta_Q$ , respectively, quantify the strength of the active stress and of the active rearrangements. Negative and positive  $\zeta_Q$  values correspond to the contractile and extensile, stress along

the direction  $\vec{n}$ . For positive  $\beta_Q$ ,  $D_a$  drives cell rearrangements where a cell junction parallel to  $\vec{n}$  shrinks and is remodeled to form a new cell junction perpendicular to  $\vec{n}$ . As above,  $-\zeta_1 \Delta\mu I$  is absorbed into the pressure term when the tissue is incompressible.

We considered a uniform and fixed signal  $\vec{n} = (0, 1)^T$ . We set  $\zeta_2 = \beta_2 = 0$  to focus on the activity induced by  $Q$ . Assuming as above that  $\theta = 0$ , Eqs. (23-25) become

$$\dot{c} = 2(1 - \nu_1)\partial_x v_x - 2\eta_1^{-1}\Gamma(c)\sinh c - \beta_Q\Delta\mu \quad (29)$$

$$\sigma_{xx} = -p + \eta\partial_x v_x + (1 - \nu_1)\Gamma(c)\sinh c + \frac{\zeta_Q}{2}\Delta\mu \quad (30)$$

$$\sigma_{yy} = -p + \eta\partial_y v_y - (1 - \nu_1)\Gamma(c)\sinh c - \frac{\zeta_Q}{2}\Delta\mu. \quad (31)$$

In isotropic stress conditions ( $\sigma_{xx} = \sigma_{yy}$ ), both the cellular shape anisotropy at steady state ( $\dot{c} = 0$ ), determined by:

$$\Gamma(c)\sinh c = -\frac{(1 - \nu_1)\eta_1\zeta_Q + \eta\eta_1\beta_Q}{\eta_1(1 - \nu_1)^2 + \eta} \frac{\Delta\mu}{2}, \quad (32)$$

and the tissue deformation rate  $\partial_x v_x$

$$\partial_x v_x = \frac{-\zeta_Q + (1 - \nu_1)\eta_1\beta_Q}{\eta_1(1 - \nu_1)^2 + \eta} \frac{\Delta\mu}{2}. \quad (33)$$

remain non-zero, indicating that the tissue anisotropy and flow are maintained through the active stresses and cell rearrangements. In Eqs. (32) and (33), cellular shape anisotropy  $c$  and velocity gradient  $\partial_x v_x$  may adopt either an identical or an opposite sign depending on the numerical values of the active coefficients  $\beta_Q$  and  $\zeta_Q$ . Therefore, cell elongation occurs either parallel or perpendicular to the direction of flow, depending on the parameter values (phase diagram in Fig. 4(b), with  $\nu_1 < 1$ ). Considering the contractile effect of myosin motors (upper right quadrant of Fig. 4(b),  $-\zeta_Q > 0$  and  $\beta_Q > 0$ ), cell elongation occurs mostly perpendicular to the tissue flow, except below the green line of the slope  $(1 - \nu_1)/\eta$ . An earlier study using the CPM suggested that the differential cell adhesion accounts for CE with cell elongation orthogonal to tissue flow, in which only the outer tissue boundary contributes to the driving of tissue deformation [64, 65]. Our model provides an alternative mechanism in which activities play an essential role, in agreement with recent observations of elevated myosin activity in the elongated cell junctions orthogonal to the tissue flow [61, 62].

### C. Shear flow

A fundamental geometry for investigating rheology [66], shear flow is commonly found in many developmental tissues [12, 53, 62]. Here, we considered the simple geometry given in Fig. 5(a), inspired by the plane Couette flow [66]. The flow, with shear rate  $\dot{\gamma} = \partial_y v_x$ , is driven by an external shear stress  $\sigma_b$  acting in the opposite directions on the boundaries. The effective shear

viscosity  $\eta_{\text{eff}} \equiv 2\sigma_b/\dot{\gamma}$  can be calculated as:

$$\eta_{\text{eff}} = \eta + (1 - \nu_1)^2 \eta_1 - (1 - \nu_1) \eta_1 \cos 2\theta \tanh c, \quad (34)$$

where the cell shape anisotropy  $c$  and orientation  $\theta$  depend on the driving stress  $\sigma_b$  (see Appendix C). In the presence of a coupling between the cellular rearrangement rate and the elastic stress ( $\eta_1 \neq 0$ ),  $\eta_{\text{eff}}$  depends on  $\sigma_b$ , which makes the tissue non-Newtonian (Fig. 5). The shear rate is an increasing function of the external stress  $\sigma_b$ , whereas the effective shear viscosity decreases with  $\dot{\gamma}$ , indicating that the model predicts shear-thinning (Fig. 5(b-c)). Cellular shape anisotropy  $c$  increases with  $\sigma_b$  or  $\dot{\gamma}$ , to converge to a finite value for large driving. Cells turn in the direction of the applied stress as they elongate (Fig. 5(d-f)). Shear-thinning was reported *in vitro*, using cellular spheroids [67], and was shown to be related to stress-dependent barriers that may control cell rearrangements (see [56] for a mechanism leading to shear-thinning in active materials that does not involve topological effects). To the best of our knowledge, there is no experimental evidence for the shear-thinning in epithelial tissues *in vivo*, which is a non-trivial prediction of our model, obtained assuming only linear force-flux couplings.

Including the active stress and active cell rearrangements, both internal, Eqs. (20-21), or due to an oriented signal, Eqs. (27-28), the shear rate becomes

$$\dot{\gamma} = 2 \frac{\sigma_b + \sigma_2 + \sigma_Q}{\eta + (1 - \nu_1)^2 \eta_1 - (1 - \nu_1) \eta_1 \cos 2\theta \tanh c}, \quad (35)$$

with  $\sigma_2 = \Delta\mu M_0 \sinh c \sin 2\theta (\zeta_2 - 2\eta_1(1 - \nu_1)\beta_2)$  and  $\sigma_Q = \Delta\mu \sin 2\phi (\zeta_Q + \eta_1(1 - \nu_1)\beta_Q)$ . In addition to the external stress  $\sigma_b$ , active stresses and active cell rearrangements are able to drive shear flow. Indeed, the active rearrangements described by Eq. (28) produce shear flow for an arbitrary orientation  $\phi$ , as has been observed in the genitalia of *Drosophila* and demonstrated using the CVM in the case of  $\vec{n}$  pointing to  $\phi = 3\pi/4$  [53].

#### IV. DISCUSSION

We formulated a two-dimensional continuum model of epithelial mechanics that treats in-plane tissue deformation in which cells deform, move and intercalate without compromising tissue cohesion. Our aim was to provide a general modeling scheme rather than a specific extension of the CVM/CPM. The functional form of the elastic energy density  $F$ , apart from the usual requirements imposed by symmetry, is free to accommodate other relevant aspects of the mechanics of tissue. For instance, specific expressions of  $F$  may allow to include non-linear elasticity, to study the dynamics of non-epithelial tissues, which fall out of the scope of the CVM, or to coarse-grain other cell-based models, including particle-based and phase-field models [20–25]. Once the functional form of the energy is formulated in terms of  $M$ , a continuum model can be derived as has been done here: the

CVM/CPM is but a possible source of inspiration to connect cell scale with tissue scale mechanics, and was chosen due to its popularity in developmental biology.

The advantages of using this approach are as follows. Most importantly, our model is designed to connect cellular level mechanical ingredients (*e.g.*, cell area elasticity and cell junction tension) and cell morphogenetic processes (*e.g.*, cell rearrangements), in order to drive tissue mechanics and deformation. This was achieved by defining the energy function and kinematic relationship in terms of the cell shape field  $M$ , which distinguishes our work from the previous continuum models [30, 33, 34]. The model describes time-dependent flows, and allows the evaluation of time scales as a function of material parameters. Large and non-affine deformations can be treated. In addition, the model can also incorporate a signal field, for instance, the axial tensor  $Q$ , which, here, orients active stresses and cellular rearrangements. The main hypotheses underlying our approach are the following: (*i*) the symmetric part of the velocity gradient tensor and of the total stress tensor can be decomposed additively, see Eqs. (1) and (15) respectively; (*ii*) the framework of linear nonequilibrium thermodynamics allows to describe epithelial mechanics. When considering applications, we assumed in addition that external forces applied on the epithelium, such as friction between the tissue and substrate, are negligible. Upon coarse-graining, possible short-range heterogeneity among cells is also lost, a point that should be kept in mind when modeling actual tissues. Many relevant fields can be experimentally determined, including tissue stress, tissue deformation, cell morphogenetic processes, and chemical signaling fields, such as the concentrations of cell polarity molecules or the orientation field describing the spatial distribution of myosin molecules. Once their dynamics are quantitatively characterized by the relevant scalar, vector, or tensor variables [5, 6, 11–13, 52, 68, 69], comparison between the model and experiments is feasible.

The results presented here demonstrate that using our model, we can predict the dynamical behaviors underlying epithelial tissue morphogenesis. In the future, the quantitative comparison of the model predictions with experimental data should help us evaluate material parameters and validate constitutive equations. For example, since  $D$ ,  $D_r$  [12] and  $\sigma_e$  [13, 14] are measurable quantities, the validity of the kinematic relationship Eq. (2) and of the constitutive relation Eq. (18) can be tested by experimental observation.

The current approach can be extended in several ways. Other cell morphogenetic processes, such as cell division and cell death, should be incorporated to the current modeling scheme [70]. Plastic behavior [67] may be considered as well, either within the dissipation function formalism [30], or by considering non-linear constitutive equations to effectively incorporate a yield stress. In analogy to the recent adaptations of the CPM [71] or the CVM [72], a cell polarity field may be included to describe collective cell migration [70]. Another possi-

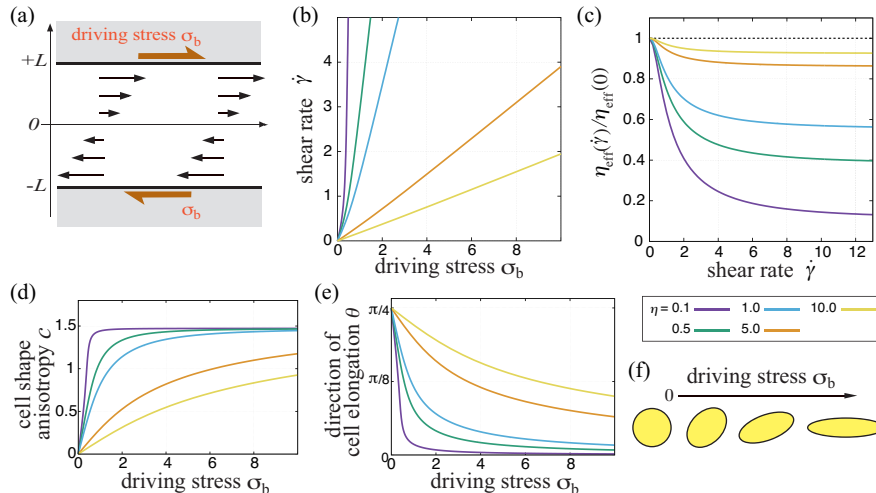


FIG. 5. The tissue behaving as a shear-thinning fluid. (a) An external shear stress ( $\sigma_b$ ) is applied at the top and bottom boundaries ( $y = \pm L$ ). (b) The shear rate  $\dot{\gamma}$  is plotted against the driving stress  $\sigma_b$ . (c) The effective viscosity  $2\sigma_b/\dot{\gamma}$  decreases as a function of the shear rate  $\dot{\gamma}$ . Cell shape anisotropy  $c$  (d) and orientation  $\theta$  (e) are plotted as a function of the driving stress  $\sigma_b$ . (f) Cells elongate and align along the force axis as the driving stress  $\sigma_b$  increases. Parameters were set as  $\gamma_0/(4M_0)^{1/2} = 0.1 \text{ mN m}^{-1}$ ,  $2\pi\kappa_0 = 0.4 \text{ mN m}^{-1}$ ,  $\nu_1 = 0.1$  and  $\eta_1 = 1.0 \text{ Pa m s}$ .

ble extension of the model concerns kinetics. Here, the associated dissipation coefficients, including the coefficients governing active stress and active rearrangement, were determined phenomenologically by employing the thermodynamic formalism. This point can be further explored by considering detailed processes at the cellular level [12, 43, 49, 52]. In particular, the cell-level machinery underlying tissue-level active processes should be studied further in connection with signal activity dynamics. Emerging spatio-temporal patterns will also be of interest. Various dynamics arise in active nematic models, which may describe cultured cell monolayers [54], and which share a common mathematical structure with the present model. Finally, our 2D formalism can be extended to 3D.

In conclusion, the present work provides an integrated scheme for the understanding of the mechanical control of epithelial morphogenesis. Dynamics of signal fields can be coupled to the equations. Feedback between biochemical signaling and mechanics through the mechanosensing of a cell [4–8] may represent a potential future research direction.

## ACKNOWLEDGMENTS

We thank Yohanns Bellaïche, Cyprien Gay, François Graner, Boris Guirao, and Shunsuke Yabunaka for discussion. This research was supported by JSPS KAKENHI Grant Number JP24657145 and JP25103008, the

JST CREST (JPMJCR13W4), the JST PRESTO program (13416135), and by the JSPS/MAEDI/MENESR Sakura program.

## Appendix A: Energy function and elastic stress

### 1. Derivation of elastic stress

The shape of a given cell is represented by  $(\vec{r} - \vec{r}_c)^T M^{-1} (\vec{r} - \vec{r}_c) = 1$ , where  $M$  is a positive definite matrix, and the center of the cell is located at  $\vec{r}_c$ .

Let each material point at the position  $\vec{r}$  move to  $\tilde{\vec{r}} = \vec{r} + \vec{u}(\vec{r})$ , thus defining the displacement field  $\vec{u}$ . The center of a cell changes as  $\tilde{\vec{r}}_c = \vec{r}_c + \vec{u}(\vec{r}_c)$  and the cell shape changes as

$$(\vec{r} - \tilde{\vec{r}}_c)^T ((1 + \nabla \vec{u})^{-1})^T M^{-1} (1 + \nabla \vec{u})^{-1} (\vec{r} - \tilde{\vec{r}}_c) = 1.$$

Upon coarse-graining, this indicates that  $M$  changes as

$$\tilde{M}(\vec{x} + \vec{u}) = (1 + \nabla \vec{u}) M(\vec{x}) (1 + \nabla \vec{u}^T),$$

whereby, at order  $\mathcal{O}(|\nabla \vec{u}|)$ ,

$$M \rightarrow \tilde{M} = M - \vec{u} \cdot \nabla M + M(\nabla \vec{u})^T + \nabla \vec{u} M. \quad (\text{A1})$$

This equation represents the relationship between the change in the cell shape and tissue displacement field, in the absence of cell rearrangements. It has been derived rigorously for a cellular material in [30].

By the virtual displacement  $\vec{u}$ , the total energy  $\tilde{F}(M) = \int F(M) d\vec{x}$  changes as follows:

$$\begin{aligned}
\delta\tilde{F} &= \tilde{F}(M') - \tilde{F}(M) \simeq \int \frac{\partial F}{\partial M} : \delta M d\vec{x} = \int \frac{\partial F}{\partial M} : (-\vec{u} \cdot \nabla M + M(\nabla\vec{u})^T + \nabla\vec{u}M) d\vec{x} \\
&= \int \left[ -\nabla \cdot (\vec{u}F) + \left( FI + \left( \frac{\partial F}{\partial M} \right)^T M + \frac{\partial F}{\partial M} M^T \right) : \nabla\vec{u} \right] d\vec{x}
\end{aligned} \tag{A2}$$

where  $\delta M = M' - M$ . The first term vanishes at the boundary of the system, and the elastic stress  $\sigma_e$  is given as Eq. (5).

## 2. Comparison of macroscopic and microscopic stress

To check the validity of coarse-graining, we conducted numerical simulations of the CVM with an energy function given by Eq. (8) in the main text [26, 46] and compared two expressions of the stress tensor.

The first one is the ‘microscopic’ expression directly calculated from the CVM [12–14]

$$\sigma^{\text{CVM}} = \frac{1}{\sum_i A_i} \left( -\sum_i P_i A_i I + \sum_{[ij]} T_{ij} \frac{\ell_{ij} \otimes \ell_{ij}}{\|\ell_{ij}\|} \right) \tag{A3}$$

where  $A_i$  is the area of cell  $i$ , and  $\ell_{ij}$  is the length of the interface between cells  $i$  and  $j$ .  $P_i$  is the pressure of the  $i$ -th cell originating from cell elasticity, and  $T_{ij}$  is the tension of cell interface  $[ij]$ .  $P_i$  and  $T_{ij}$  are determined from the energy function (8) as  $P_i = -K(A_i - A_0)$  and  $T_{ij} = \gamma_0 + \kappa_0(L_i + L_j)$ .

The second one is the ‘macroscopic’ expression of stress as a function of the coarse-grained cell shape tensor  $M$ , Eq. (13), estimated from the given geometry of cells in a CVM simulation. In practice, we calculated the centroid and the second moment  $\mu_2^i$  of a two dimensional region occupied by each polygon (cell)  $i$  [73], and then averaged it over  $N$  cells:

$$M = \frac{4}{N} \sum_i \mu_2^i = \frac{4}{N} \sum_i \begin{pmatrix} \mu_{2,xx}^i & \mu_{2,xy}^i \\ \mu_{2,yx}^i & \mu_{2,yy}^i \end{pmatrix} \tag{A4}$$

The factor 4 is needed since the second moment of an ellipse with major and minor radii  $a$  and  $b$  has eigenvalues  $a^2/4$  and  $b^2/4$ . With the estimated  $M$ , we calculated the cell area as  $\pi|M|^{1/2}$ , and the cell perimeter by using Euler’s formula for the ellipse perimeter truncated to second order [47]:

$$L(M) = c_h \pi \sqrt{2\text{Tr} M} \left[ 1 - \frac{1}{16} \left( 1 - \frac{4|M|}{(\text{Tr} M)^2} \right) \right] \tag{A5}$$

Agreement between the two expressions improves slightly when taking into account the ratio  $c_h = \sqrt{2\sqrt{3}/\pi} \sim 1.05$  between the perimeters of a circle and an hexagon with

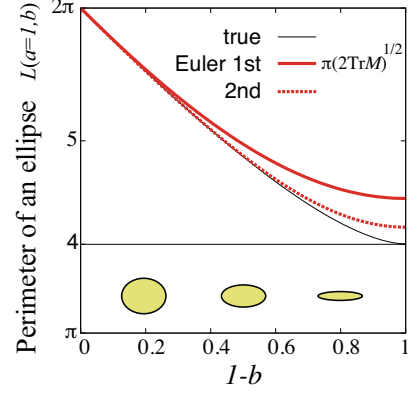


FIG. S1. Euler approximation of the perimeter  $L$  of an ellipse of semi-axes  $a = 1$  and  $b \in [0, 1]$  as a function of  $1 - b$  at first and second order is compared to the exact value. The isotropic case corresponds to  $a = b$ , or  $1 - b = 0$ .

the same area. The precision of Euler’s expansion for the ellipse perimeter is illustrated in Fig. S1.

CVM simulations were conducted by minimising the energy Eq. (8). An external stress  $\sigma^{\text{ex}}$  was applied on the boundary of the system, for which we took  $\sigma_{xy}^{\text{ex}} = \sigma_{yx}^{\text{ex}} = \sigma_{yy}^{\text{ex}} = 0$ , while  $\sigma_{xx}^{\text{ex}}$  was controlled to stretch the system along the  $x$ -axis. After the system relaxed, we confirmed that the force was balanced and that the stress  $\sigma^{\text{CVM}}$  converged to coincide with the external stress  $\sigma^{\text{ex}}$ . We distinguish the stress that comes from cell elasticity ( $-P^{\text{ce}} I$ , where  $P^{\text{ce}}$  denotes the pressure) and from cell junction tension ( $\sigma^{\text{T}}$ ), respectively (*i.e.*, the first and the second terms of Eqs. (A3) and (13)). In the simulations, parameters are set as  $K = 10.0$ ,  $A_0 = 1.0$  and  $\kappa_0/K A_0 = 0.02, 0.04$ . The results are summarized in Fig. 2(a,b) in the main text and detailed in Fig. S2.

The values found for the macroscopic expression of stress with coarse-grained cell shape  $M$  agree well with the microscopic (correct) stress, as long as the cell aspect ratio is not too large.

## 3. Stability analysis of the energy function

*a. Cell area instability* Let cell shape be uniform, not depending on the position  $\vec{r}$ . With the expression  $M = M_0 e^{c\Theta}$ , the cell area reads  $A = \pi M_0$ , and the energy density function per cell,  $f = A F(M)$ , is expressed

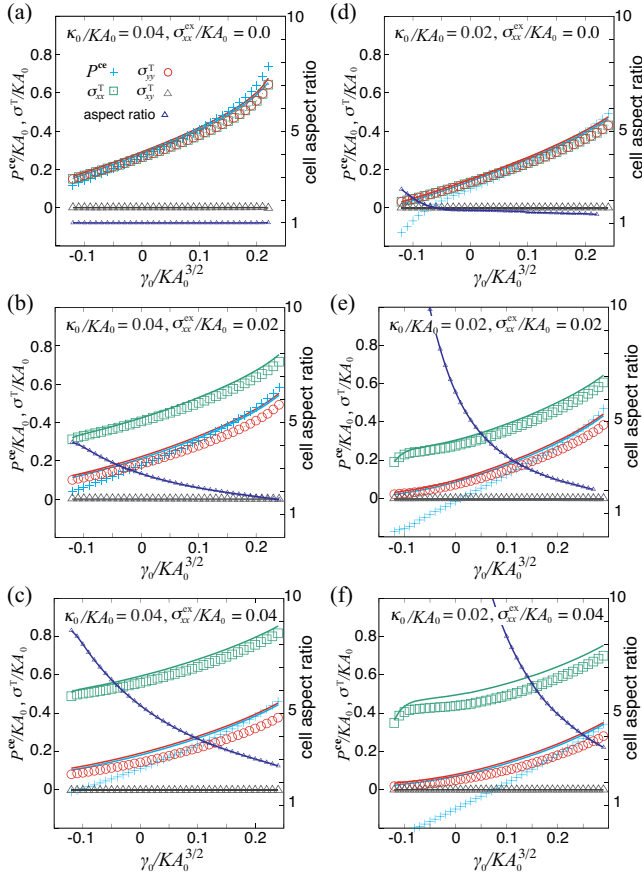


FIG. S2. Macroscopic stress expressions calculated from coarse-grained cell shape tensor  $M$  (symbols) are compared with the true ones (solid lines) obtained by CVM simulations (left vertical axis), as a function of the non-dimensionalized parameter  $\gamma_0 / K A_0^{3/2}$ , with  $\kappa_0 / K A_0 = 0.02$  (right column) and  $\kappa_0 / K A_0 = 0.04$  (left column).  $P^{ce}$  and  $\sigma^T$  are the pressure and stresses originating from cell elasticity and cell junction tensions, respectively. Blue triangles denote the mean cell shape aspect ratio (right vertical axis), equal to  $\exp(2c)$  in terms of the cell shape anisotropy. A green solid line overlaps with a red one and does not appear in (a) and (d). Components of the external stress are set as  $\sigma_{xy}^{ex} = \sigma_{yy}^{ex} = 0$ , with (from left to right column)  $\sigma_{xx}^{ex} = 0.0, 0.02, 0.04$ .

as

$$f = \frac{K}{2} (\pi M_0 - A_0)^2 + \pi \gamma_0 \sqrt{M_0} \cosh c + 2\pi^2 \kappa_0 M_0 \cosh c \quad (\text{A6})$$

The pressure  $P$  is obtained by differentiating  $f$  with respect to  $A = \pi M_0$  (equivalently  $P = -\text{Tr} \sigma_e / 2$ )

$$P = -K(\pi M_0 - A_0) - \frac{\gamma_0}{2} \sqrt{\frac{\cosh c}{M_0}} - 2\pi \kappa_0 \cosh c. \quad (\text{A7})$$

Thermodynamic stability holds when  $\partial P / \partial A < 0$ , which leads to the following condition:

$$\bar{\gamma}_0 \equiv \frac{\gamma_0}{K A^{3/2}} < \frac{4}{\pi^{1/2} \cosh c} \quad (\text{A8})$$

Note that  $\cosh c \geq 1$ , where the equality holds at  $c = 0$ . The cell area  $A$  depends on parameters and boundary conditions. For a given cell area, the described condition does not hold for large  $\gamma_0$  values, indicating that the homogenous cell size state becomes unstable. Taking higher order terms into account when approximating the ellipse perimeter does not change the condition.

*b. Cell shape instability* Since  $f$  is an even function of  $c$ , its Taylor expansion reads  $f(c) = f(0) + \frac{f''(0)}{2!} c^2 + \frac{f^{(4)}(0)}{4!} c^4 + \dots$ , with  $f''(0) = \pi \frac{\gamma_0}{2} \sqrt{M_0} + 2\pi^2 \kappa_0 M_0$ . As long as  $f''(0) > 0$ , *i.e.*,  $\gamma_0 > -4\kappa_0 \pi M_0^{1/2}$ ,  $f$  takes its minimal value at  $c = 0$ . If  $\gamma_0$  is smaller than the threshold value  $-4\kappa_0 \pi M_0^{1/2}$ , the circular shape is no longer stable, and cells preferentially take an elongated shape. Using a non-dimensionalized parameter  $\bar{\kappa}_0 = \kappa_0 / K A$ , the above condition can be written as

$$\bar{\gamma}_0 > -4\pi^{1/2} \bar{\kappa}_0 \quad (\text{A9})$$

This condition is unchanged when higher order correction of ellipse perimeter is taken into account.

## Appendix B: Hydrodynamic equations of epithelial mechanics

### 1. Constitutive equations

Including lowest-order non-linearities, with the condition that  $D_r$  is traceless, the generic form of the force-flux relationships can be written as:

$$\begin{aligned} \sigma_p &= \eta D' + \eta' (\text{Tr} D) I \\ &+ \mu (DM' + M'D) + \mu' (\text{Tr} D) M' + \mu'' (\text{Tr} (DM')) I \\ &- \nu_1 \sigma_e' - \nu_2 (\sigma_e' M' + M' \sigma_e') - \nu_3 (\sigma_e' : M') I \\ &- \zeta_1 \Delta \mu I - \zeta_2 \Delta \mu M', \end{aligned} \quad (\text{B1})$$

$$\begin{aligned} D_r &= \nu_1 D' + \nu_2 (DM' + M'D - \text{Tr} (DM') I) + \nu_3 (\text{Tr} D) M' \\ &+ \eta_1^{-1} \sigma_e' + \eta_2^{-1} (\sigma_e' M' + M' \sigma_e' - \text{Tr} (\sigma_e' M') I) \\ &- \beta_2 \Delta \mu M', \end{aligned} \quad (\text{B2})$$

where the coupling coefficients are scalar in an isotropic system (compare with Eqs. (20-21)). Note that the results of Secs. III A-III B are unchanged when using Eqs. (B1-B2) instead of Eqs (20-21), since the  $M$ -dependent terms in (B1-B2) either cancel, or are isotropic tensors that may be absorbed into the pressure.

To obtain Eqs. (B1) and (B2), we set the fourth-order tensors  $\chi^{sr}$  and  $\chi^{rr}$  as follows:

$$\chi_{ijkl}^{ss} = \eta \delta_{ik} \delta_{jl} + \eta' \delta_{ij} \delta_{kl} + \mu (\delta_{ik} M'_{lj} + M'_{ik} \delta_{jl}) + \mu' M'_{ij} \delta_{kl} + \mu'' M'_{lk} \delta_{ij} \quad (\text{B3})$$

$$\chi_{ijkl}^{sr} = \nu_1 \left( \delta_{ik} \delta_{lj} - \frac{1}{2} \delta_{ij} \delta_{kl} \right) + \nu_2 (\delta_{ik} M'_{lj} + M'_{ik} \delta_{jl} - M'_{ij} \delta_{kl}) + \nu_3 M'_{kl} \delta_{ij} \quad (\text{B4})$$

$$\chi_{ijkl}^{rs} = \nu_1 \left( \delta_{ik} \delta_{lj} - \frac{1}{2} \delta_{ij} \delta_{kl} \right) + \nu_2 (\delta_{ik} M'_{lj} + M'_{ik} \delta_{jl} - \delta_{ij} M'_{kl}) + \nu_3 \delta_{kl} M'_{ij} \quad (\text{B5})$$

$$\chi_{ijkl}^{rr} = \eta_1^{-1} \delta_{ik} \delta_{jl} + \eta_2^{-1} (\delta_{ik} M'_{lj} + M'_{ik} \delta_{jl} - M'_{lk} \delta_{ij}), \quad (\text{B6})$$

Here  $\delta_{ij}$  is the Kronecker tensor. Onsager's reciprocity  $\chi_{ijkl}^{rs} = \chi_{klij}^{sr}$  is satisfied.

## 2. Incompressible flow

An incompressible flow is characterized by a constant  $|M|$ , and thus  $\nabla \cdot \vec{v} = 0$  according to Eq. (3). The factorization  $M = M_0 e^{c\Theta}$  is all the more useful since  $M_0$  is constant. The constitutive equations are replaced by

$$\sigma = \sigma'_e + \sigma'_p - pI \quad (\text{B7})$$

with

$$\sigma'_e = \left( \frac{\gamma_0}{\sqrt{2\text{Tr} M}} + 2\pi\kappa_0 \right) \frac{M'}{|M|^{1/2}}, \quad (\text{B8})$$

$$\sigma'_p = \eta D' + \mu (DM' + M'D - \text{Tr}(DM')I) - \nu_1 \sigma'_e - \nu_2 (\sigma'_e M' + M' \sigma'_e) - \zeta_2 \Delta \mu M' \quad (\text{B9})$$

$$D_r = \nu_1 D + \nu_2 (DM' + M'D - \text{Tr}(DM')I) + \eta_1^{-1} \sigma'_e + \eta_2^{-1} (\sigma'_e M' + M' \sigma'_e - \text{Tr}(\sigma'_e M')I) - \beta_2 \Delta \mu M', \quad (\text{B10})$$

where  $p$  represents the tissue pressure.

## Appendix C: Shear flow

We will consider shear flow for which three kinds of driving are taken into account. The first is a shear stress acting on the boundary, the other two are the cell-intrinsic active stresses and rearrangements. Cell vertex model simulations have shown that directed cell rearrangements may produce self-driven shear flow [53]. In addition, the properties predicted by the following analysis will give opportunities to test the model in the future.

We look for a solution with steady and uniform shear velocity gradient in the form of

$$\nabla \vec{v} = \begin{pmatrix} 0 & \dot{\gamma} \\ 0 & 0 \end{pmatrix}. \quad (\text{C1})$$

In the incompressible case,  $\sigma'_e$ ,  $\sigma'_p$ , and  $D_r$  are given as

follows

$$\sigma'_e = \left( \frac{\gamma_0}{\sqrt{2\text{Tr} M}} + 2\pi\kappa_0 \right) \frac{M'}{M_0} = \Gamma(c) \sinh(c) \Theta, \quad (\text{C2})$$

$$\sigma'_p = \eta D' - \nu_1 \sigma'_e - \zeta_2 \Delta \mu M' - \zeta_Q \Delta \mu Q, \quad (\text{C3})$$

$$D_r = \nu_1 D' + \eta_1^{-1} \sigma'_e - \beta_2 \Delta \mu M' - \beta_Q \Delta \mu Q. \quad (\text{C4})$$

Here, for simplicity, we omit possible dependences of the coefficients  $\chi^{ss}$ ,  $\chi^{sr}$ ,  $\chi^{rs}$ , and  $\chi^{rr}$  on  $M'$ . With an orientation along  $\vec{n} = (\cos \phi, \sin \phi)^T$ , the external signal reads

$$Q = \frac{1}{2} \begin{pmatrix} \cos 2\phi & \sin 2\phi \\ \sin 2\phi & -\cos 2\phi \end{pmatrix}. \quad (\text{C5})$$

Writing  $D_r$  as

$$D_r = \begin{pmatrix} d_r & \delta_r \\ \delta_r & -d_r \end{pmatrix}, \quad (\text{C6})$$

$d_r$  and  $\delta_r$  are given as follows

$$d_r = \left( \frac{\Gamma(c)}{\eta_1} - \beta_2 \Delta \mu M_0 \right) \sinh c \cos 2\theta - \frac{\beta_Q \Delta \mu}{2} \cos 2\phi, \quad (\text{C7})$$

$$\delta_r = \frac{\nu_1}{2} \dot{\gamma} + \left( \frac{\Gamma(c)}{\eta_1} - \beta_2 \Delta \mu M_0 \right) \sinh c \sin 2\theta - \frac{\beta_Q \Delta \mu}{2} \sin 2\phi. \quad (\text{C8})$$

The kinematic equation at steady state ( $\dot{M} = (\nabla \vec{v} - D_r)M + M(\nabla \vec{v} - D_r)^T = 0$ ) leads to

$$(\cosh c + \sinh c \cos 2\theta) d_r = \sinh c \sin 2\theta (\dot{\gamma} - \delta_r) \quad (\text{C9})$$

$$\cosh c (\dot{\gamma} - 2\delta_r) = \dot{\gamma} \cos 2\theta \sinh c \quad (\text{C10})$$

$$(\cosh c - \sinh c \cos 2\theta) d_r = \sinh c \sin 2\theta \delta_r \quad (\text{C11})$$

One of these three equations is not independent of the others, since  $|M|$  is constant. With some calculation, we derive two independent equations

$$\dot{\gamma} - 2\delta_r = \dot{\gamma} \cos 2\theta \tanh(c) \quad (\text{C12})$$

$$2d_r = \dot{\gamma} \tanh(c) \sin 2\theta \quad (\text{C13})$$

By substituting Eqs. (C7) and (C8), we reach the equations

$$2 \left( \frac{\Gamma(c)}{\eta_1} - \beta_2 \Delta\mu M_0 \right) \sinh c \sin 2\theta - \beta_Q \Delta\mu \sin 2\phi = (1 - \nu_1 - \tanh c \cos 2\theta) \dot{\gamma} \quad (\text{C14})$$

$$2 \left( \frac{\Gamma(c)}{\eta_1} - \beta_2 \Delta\mu M_0 \right) \sinh c \cos 2\theta - \beta_Q \Delta\mu \cos 2\phi = \tanh c \sin 2\theta \dot{\gamma}, \quad (\text{C15})$$

$$\sigma = (1 - \nu_1) \Gamma(c) \sinh c \Theta + \eta D' - \zeta_2 \Delta\mu M' - \zeta_Q \Delta\mu Q - pI. \quad (\text{C16})$$

The first and second equations determine cell shape  $(c, \theta)$  for a given shear rate  $\dot{\gamma}$ , while the third equation represents the total stress  $\sigma = \sigma'_e + \sigma'_p - pI$ . The stress bound-

ary condition at  $y = +L$  (top) is given as  $\sigma_{xy} = \sigma_b$ , where  $\sigma_b$  is the force per unit length applied at the boundary to drive the shear flow. This condition reads

$$\sigma_b + \frac{\zeta_Q \Delta\mu}{2} \sin 2\phi = \frac{\eta}{2} \dot{\gamma} + (1 - \nu_1) \Gamma(c) \sinh c \sin 2\theta - \zeta_2 \Delta\mu M_0 \sinh c \sin 2\theta \quad (\text{C17})$$

The active stress  $\zeta_Q \Delta\mu \sin 2\phi/2$  plays a role equivalent to the external driving stress  $\sigma_b$  in the sense that it shifts

$\sigma_b$  by a constant as  $\sigma'_b = \sigma_b - \zeta_Q \Delta\mu \sin 2\phi/2$ .

From Eqs. (C14), (C15) and (C17), we can evaluate how the shear rate  $\dot{\gamma}$  depends on the driving stress  $\sigma_b$ .

$$\dot{\gamma} = 2 \frac{\sigma_b + \Delta\mu ((\zeta_Q - (1 - \nu_1)\eta_1\beta_Q) \sin 2\phi + (\zeta_2 - 2\eta_1(1 - \nu_1)\beta_2)M_0 \sinh c \sin 2\theta)}{\eta + (1 - \nu_1)\eta_1 [1 - \nu_1 - \tanh c \cos 2\theta]} \quad (\text{C18})$$

For  $\sigma_b = \zeta_Q = \beta_2 = \zeta_2 = 0$ , Eq. (C18) shows that oriented active rearrangements suffice to generate shear flow, as shown using the CVM in [53] with an orientation along  $\vec{n} = (-1/\sqrt{2}, 1/\sqrt{2})$ , with  $\phi = 3\pi/4$ , and an external signal

$$Q = \frac{1}{2} \begin{pmatrix} 0 & -1 \\ -1 & 0 \end{pmatrix}. \quad (\text{C19})$$

For  $\Delta\mu = 0$ ,  $\eta_{\text{eff}} = 2\sigma_b/\dot{\gamma}$  is not constant, indicating that the tissue is a non-Newtonian material (Fig. 5(b-c) in the main text). As  $\sigma_b$  and accordingly  $\dot{\gamma}$  increase,  $\eta_{\text{eff}}$  converges to  $\eta_{\text{eff}}^\infty = \eta$  (Fig. 5(c)). This convergence occurs at the rate  $\eta_{\text{eff}} - \eta \sim \dot{\gamma}^{-2}$ , as shown in the numerical calculation (Fig.S3).

To understand this dependence of  $\eta_{\text{eff}}$  on  $\dot{\gamma}$ , let us consider Eqs. (C14) and (C15) with  $\Delta\mu = 0$ .

$$2\Gamma(c) \sinh c \sin 2\theta = \eta_1 (1 - \nu_1 - \tanh c \cos 2\theta) \dot{\gamma} \quad (\text{C20})$$

$$2\Gamma(c) \sinh c \cos 2\theta = \eta_1 \tanh c \sin 2\theta \dot{\gamma} \quad (\text{C21})$$

For the right hand sides of these equations to remain finite in the limit  $\dot{\gamma} \rightarrow \infty$ ,  $c$  and  $\theta$  converge to  $c \rightarrow c^\infty$  and  $\theta \sim \dot{\gamma}^{-1} \rightarrow 0$ , respectively, where  $c^\infty$  is a solution of the following equation:

$$\tanh c^\infty = 1 - \nu_1. \quad (\text{C22})$$

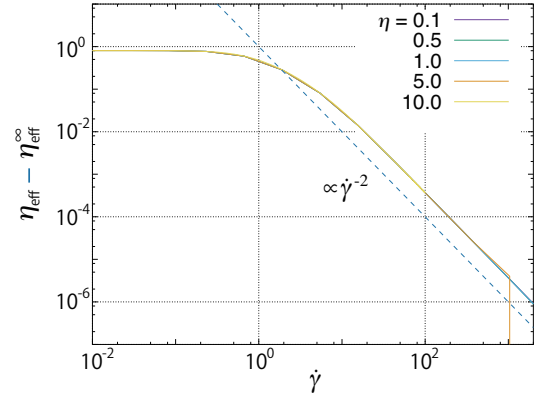


FIG. S3. Log-log plot of the difference  $\eta_{\text{eff}} - \eta_{\text{eff}}^\infty$  as a function of the shear rate  $\dot{\gamma}$ . The dashed line corresponds to  $\eta_{\text{eff}} - \eta_{\text{eff}}^\infty \propto \dot{\gamma}^{-2}$ .

Considering small deviations  $c = c^\infty - \Delta c$  and  $\theta = \Delta\theta$ , Eq. (C20) reads

$$4\Gamma(c^\infty) \sinh c^\infty \Delta\theta = \frac{\Delta c}{\cosh^2 c^\infty} \dot{\gamma}, \quad (\text{C23})$$

thus  $\Delta c$  is of the order of  $\Delta c \sim \dot{\gamma}^{-2}$ . The difference

$\eta_{\text{eff}} - \eta$  for large  $\dot{\gamma}$  is evaluated from Eq. (C18), as

$$\begin{aligned}\eta_{\text{eff}} - \eta &= (1 - \nu_1)\eta_1 [1 - \nu_1 - \tanh c \cos 2\theta] \\ &\sim (1 - \nu_1)\eta_1 \frac{\Delta c}{\cosh^2 c^\infty} \\ &\sim \eta_1 \nu_1 (1 - \nu_1) (2 - \nu_1) \Delta c,\end{aligned}\quad (\text{C24})$$

which is of the order of  $\dot{\gamma}^{-2}$ .

- 
- [1] C.P. Heisenberg, Y. Bellaïche, *Forces in tissue morphogenesis and patterning*, Cell **153**, 948 (2013).
- [2] Sampathkumar A, Yan A, Krupinski P, Meyerowitz EM, *Physical forces regulate plant development and morphogenesis*, Curr. Biol. **24**, R475-R483 (2014).
- [3] T. Lecuit, P.F. Lenne, E. Munro, *Force generation, transmission, and integration during cell and tissue morphogenesis*, Annu. Rev. Cell Dev. Biol. **27**, 157 (2011).
- [4] G.B. Blanchard, R.J. Adams, *Measuring the multi-scale integration of mechanical forces during morphogenesis*, Curr. Opin. Genet. Dev. **21**, 653 (2011).
- [5] Aigouy B, et al., *Cell flow reorients the axis of planar polarity in the wing epithelium of Drosophila*, Cell **142**, 773 (2010).
- [6] K. Sugimura, S. Ishihara, *The mechanical anisotropy in a tissue promotes ordering in hexagonal cell packing*, Development **140**, 4091 (2013).
- [7] W.Y. Aw, B.W. Heck, B. Joyce, D. Devenport, *Transient tissue-scale deformation coordinates alignment of planar cell polarity junctions in the mammalian skin*, Curr. Biol. **26**, 2090 (2016).
- [8] M. Uyttewaal, et al., *Mechanical stress acts via Katanin to amplify differences in growth rate between adjacent cells in Arabidopsis*, Cell **149**, 439 (2012).
- [9] T. Schluck, U. Nienhaus, T. Aegerter-Wilmsen, C.M. Aegerter, *Mechanical control of organ size in the development of the Drosophila wing disc*, PLoS One **8**, e76171 (2013).
- [10] T.P. Wyatt, et al., *Emergence of homeostatic epithelial packing and stress dissipation through divisions oriented along the long cell axis*, Proc. Nat. Acad. Sci. USA **112**, 5726 (2015).
- [11] F. Bosveld, et al., *Mechanical control of morphogenesis by Fat/Dachsous/Four-jointed planar cell polarity pathway*, Science **336**, 724 (2012).
- [12] B. Guirao, S. U. Rigaud, F. Bosveld, A. Bailles, J. Lopez-Gay, S. Ishihara, K. Sugimura, F. Graner, and Y. Bellaïche, *Unified quantitative characterization of epithelial tissue development*, eLife **4**, e08519 (2015).
- [13] S. Ishihara, K. Sugimura, *Bayesian inference of force dynamics during morphogenesis*, J. Theor. Biol. **313**, 201 (2012).
- [14] S. Ishihara, K. Sugimura, S. J. Cox, I. Bonnet, Y. Bellaïche, and F. Graner, *Comparative study of non-invasive force and stress inference methods in tissue*, Eur. Phys. J. E **36**, 45 (2013).
- [15] K.K. Chiou, L. Hufnagel, B.I. Shraiman, *Mechanical stress inference for two dimensional cell arrays*, PLoS Comput. Biol. **8**, e1002512 (2012).
- [16] G.W. Brodland GW, et al., *CellFIT: A cellular force-inference toolkit using curvilinear cell boundaries*, PLoS One **9**, e99116 (2014).
- [17] N. Khalilgharibi, J. Fouchard, P. Recho, G. Charras, A. Kabla, *The dynamic mechanical properties of cellularised aggregates*, Curr. Opin. Cell Biol. **42**, 113 (2016).
- [18] H. Honda, *Geometrical models for cells in tissues*, Int. Rev. Cytol. **81**, 191 (1983).
- [19] F. Graner, Y. Sawada *Can surface adhesion drive cell rearrangement? part II: A geometrical model*, J. Theor. Biol. **164**, 477 (1993).
- [20] D. Drasdo and S. Höhme, *A single-cell-based model of tumor growth in vitro: monolayers and spheroids*, Phys. Biol. **2**, 133 (2005).
- [21] M. Basan, J. Prost, J.-F. Joanny, J. Elgeti, *Dissipative particle dynamics simulations for biological tissues: rheology and competition*, Phys. Biol. **8**, 026014 (2011).
- [22] S.A. Sandersius, C.J. Weijer, T.J. Newman, *Emergent cell and tissue dynamics from subcellular modeling of active biomechanical processes*, Phys. Biol. **8**, 045007 (2011).
- [23] M. Nonomura, *Study on Multicellular Systems Using a Phase Field Model*, PLoS One, **7**, e33501 (2012).
- [24] B.A. Camley et al. *Polarity mechanisms such as contact inhibition of locomotion regulate persistent rotational motion of mammalian cells on micropatterns* Proc. Nat. Acad. Sci. U.S.A, **111**, 14770 (2014).
- [25] J. Löber, F. Ziebert, and I.S. Aranson, *Collisions of deformable cells lead to collective migration*, Sci. Rep. **5**, 9172 (2015).
- [26] A.G. Fletcher, M. Osterfield, R.E. Baker, S.Y. Shvartsman, *Vertex models of epithelial morphogenesis*, Biophys. J. **106**, 2291 (2014).
- [27] A.F.M. Marée, V.A. Grieneisen, P. Hogeweg, *The cellular Potts model and biophysical properties of cells, tissues and morphogenesis Single-Cell-Based Models in Biology and Medicine*, eds Anderson ARA, Chaplain MAJ, Rejniak KA Springer-Verlag, New York, (2007).
- [28] G.W. Brodland *Computational modeling of cell sorting, tissue engulfment, and related phenomena: A review*, Appl. Mech. Rev. **57**, 47 (2004).
- [29] Y. C. Fung *Biomechanics mechanical properties of living tissues 2nd ed.*, Springer-Verlag, New York (1993).
- [30] S. Tlili, et al. *Mechanical formalisms for tissue dynamics*, Eur. Phys. J. E Soft Matter **38**, 121 (2015).
- [31] B.I. Shraiman, *Mechanical feedback as a possible regulator of tissue growth*, Proc. Nat. Acad. Sci. USA **102**, 3318 (2005).
- [32] J. Ranft, et al., *Fluidization of tissues by cell division and apoptosis*, Proc. Nat. Acad. Sci. USA **107**, 20863-20868 (2010).
- [33] Popović M, et al., *Active dynamics of tissue shear flow*,

New J. Phys. **19**, 033006 (2017).

- [34] G.W. Brodland, D.I.L. Chen, J.H. Veldhuis, *A cell-based constitutive model for embryonic epithelia and other planar aggregates of biological cells*, Int. J. Plast. **22**, 965 (2006).
- [35] N. Murisic, V. Hakim, I.G. Kevrekidis, S.Y. Shvartsman, B. Audoly, *From discrete to continuum models of three-dimensional deformations in epithelial sheets*, Biophys. J. **109**, 154 (2015).
- [36] S. Turner, *Using cell potential energy to model the dynamics of adhesive biological cells*, Phys. Rev. E **71**, 041903 (2005).
- [37] J.A. Fozard, H.M. Byrne, O.E. Jensen, J.R. King, *Continuum approximations of individual-based models for epithelial monolayers*, Math. Med. Biol. **27**, 39 (2010).
- [38] J.G. Oldroyd, *On the formulation of rheological equations of state*, Proc. Roy. Soc. A **200**, 523 (1950).
- [39] R.G. Larson, *Convection and diffusion of polymer network*, J. Non-Newtonian Fluid Mech. **13**, 279 (1983).
- [40] R.G. Larson, *Constitutive Equations for Polymer Melts and Solutions*, Butterworth-Heinemann (1988).
- [41] A.I. Leonov, *Nonequilibrium thermodynamics and rheology of viscoelastic polymer media*, Rheological Acta **15**, 85 (1976).
- [42] A.I. Leonov, *On a class of constitutive equations for viscoelastic liquids*, J. Non-Newtonian Fluid Mech. **25**, 1 (1987).
- [43] F. Graner, B. Dollet, C. Raufaste, P. Marmottant, *Discrete rearranging disordered patterns, part I: Robust statistical tools in two or three dimensions* Eur. Phys. J. E **25**, 349 (2009).
- [44] P. Marmottant, C. Raufaste, F. Graner, *Discrete rearranging disordered patterns, part II: 2D plasticity, elasticity and flow of a foam*, Eur. Phys. J. E **25**, 371 (2008).
- [45] S. Bénito, C.H. Bruneau, T. Colin, C. Gay, F. Molino, *An elasto-visco-plastic model for immortal foams or emulsions*, Eur. Phys. J. E **25**, 225 (2008).
- [46] R. Farhadifar, J.C. Röper, B. Aigouy, S. Eaton, F. Jülicher, *The influence of cell mechanics, cell-cell interactions, and proliferation on epithelial packing*, Curr. Biol. **17**, 2095 (2007).
- [47] T.R. Chandrupatla, *The perimeter of an ellipse*, Math. Scientist **35**, 122 (2010).
- [48] G.K. Batchelor, *The stress system in a suspension of force-free particles*, J. Fluid Mech. **41**, 545 (1970).
- [49] M. Merkel, et al., *Triangles bridge the scales: Quantifying cellular contributions to tissue deformation*, Phys. Rev. E **95**, 032401 (2017).
- [50] D.B. Staple, et al., *Mechanics and remodelling of cell packings in epithelia*, Eur. Phys. J. E **33**, 117 (2010).
- [51] S.R. De Groot, P. Mazur, *Non-equilibrium thermodynamics*, North-Holland Publishing Company, Amsterdam (1962).
- [52] R. Etoynay, et al., *Interplay of cell dynamics and epithelial tension during morphogenesis of the drosophila pupal wing*, eLife **4**, e14334 (2015).
- [53] K. Sato, et al., *Left-right asymmetric cell intercalation drives directional collective cell movement in epithelial morphogenesis*, Nat. Comm. **6**, 10074 (2015).
- [54] Saw TB, et al., *Topological defects in epithelia govern cell death and extrusion*, Nature **544**, 212 (2017).
- [55] K. Kruse, J.F. Joanny, F. Jülicher, J. Prost, K. Sekimoto K., *Generic theory of active polar gels: a paradigm for cytoskeletal dynamics*, Eur. Phys. J. E **16**, 5 (2005).
- [56] M.C. Marchetti, et al., *Hydrodynamics of soft active matter*, Rev. Mod. Phys. **85**, 1143 (2013).
- [57] K. Bambardekar, R. Clément, O. Blanc, C. Chardès, P.F. Lenne, *Direct laser manipulation reveals the mechanics of cell contacts in vivo*, Proc. Nat. Acad. Sci. USA **112**, 1416 (2015).
- [58] K. Guevorkian, M.J. Colbert, M. Durth, S. Dufour, F. Brochard-Wyart, *Aspiration of biological viscoelastic drops*, Phys. Rev. Lett. **104**, 218101 (2010).
- [59] T.V. Stirbat, et al., *Fine tuning of tissues' viscosity and surface tension through contractility suggests a new role for  $\alpha$ -catenin*, PLoS One **8**, e52554 (2013).
- [60] M. Tada, C.P. Heisenberg, *Convergent extension: using collective cell migration and cell intercalation to shape embryos*, Development **139**, 3897 (2012).
- [61] A. Shindo, J.B. Wallingford *PCP and septins compartmentalize cortical actomyosin to direct collective cell movement*, Science **343**, 649 (2014).
- [62] E. Rozbicki, et al., *Myosin-II-mediated cell shape changes and cell intercalation contribute to primitive streak formation*, Nat. Cell Biol. **17**, 397 (2015).
- [63] Y. Morishita, K. Hironaka, S. Lee, T. Jin, D. Ohtsuka, *Reconstructing 3D deformation dynamics for curved epithelial sheet morphogenesis from positional data of sparsely-labelled cells*, Nat. Commun. **18**, 15 (2017).
- [64] M. Zajac, G.L. Jones, J.A. Glazier, *Model of convergent extension in animal morphogenesis*, Phys. Rev. Lett. **85**, 2022 (2000).
- [65] M. Zajac, G.L. Jones, J.A. Glazier, *Simulating convergent extension by way of anisotropic differential adhesion*, J. Theor. Biol. **222**, 247 (2003).
- [66] P. Oswald, *Rheophysics: The Deformation and Flow of Matter*, Cambridge University Press, UK (2009).
- [67] P. Marmottant, et al., *The role of fluctuations and stress on the effective viscosity of cell aggregates*, Proc. Nat. Acad. Sci. USA **106**, 17271 (2009).
- [68] G.B. Blanchard, et al., *Tissue tectonics: morphogenetic strain rates, cell shape change and intercalation*, Nat. Methods **6**, 458 (2009).
- [69] G. B. Blanchard, *Taking the strain: quantifying the contributions of all cell behaviours to changes in epithelial shape*, Phil. Trans. Roy. Soc. B **372**, 20150513 (2017).
- [70] S. Yabunaka and P. Marcq, *Cell growth, division and death in cohesive tissues: a thermodynamic approach*, Phys. Rev. E **96**, 022406 (2017)
- [71] A.J. Kabla, *Collective cell migration: leadership, invasion and segregation*, J. R. Soc. Interface **9**, 3268 (2012).
- [72] D.L. Barton, S. Henkes, C.J. Weijer, R. Sknepnek, *Active vertex model for cell-resolution description of epithelial tissue mechanics*, BioRxiv doi: <https://doi.org/10.1101/095133> (2016).
- [73] C. Steger, *On the Calculation of Arbitrary Moments of Polygons*, Technical Report FGBV-96-05, Technische Universität München (1996).